gastroenterology insights

MDPI

Review

CT and MR Imaging of Hepatocellular Carcinoma and Liver Cirrhosis

Masahiro Okada [1,*], Ryoji Aoki [1], Yujiro Nakazawa [1], Kenichiro Tago [1] and Kazushi Numata [2]

[1] Department of Radiology, Nihon University School of Medicine, 30-1 Ohyaguchi-kamicho, Itabashi-ku, Tokyo 173-8610, Japan; aoki.ryoji@nihon-u.ac.jp (R.A.); y.nakazawa@rad.med.keio.ac.jp (Y.N.); tago.kenichiro@nihon-u.ac.jp (K.T.)

[2] Gastroenterological Center, Yokohama City University Medical Center, 4-57 Urafune-cho, Minami-ku, Yokohama 232-0024, Japan; kz_numa@yokohama-cu.ac.jp

* Correspondence: okada.masahiro@nihon-u.ac.jp

Abstract: Liver masses are routinely evaluated using ultrasonography (US), computed tomography (CT), and magnetic resonance imaging (MRI). MRI may be used for further investigation in cases with atypical findings and difficult diagnoses. Hepatocellular carcinoma (HCC) is a common malignancy, and it is important to know the exact spread and number of HCCs, as there are numerous treatment options. In addition, it is important to know how the differentiations of HCCs are reflected on the images, and what the subtypes of HCCs look like on the images. Elastography with US and MRI is increasingly used to measure liver stiffness, and non-invasive assessment of liver fibrosis is also possible. This review describes the diagnosis of HCC on commonly used CT and MRI, and also touches on the frontiers of imaging diagnosis of liver parenchymal changes such as liver cirrhosis.

Keywords: liver tumor; liver cirrhosis; MRI; CT; MR elastography

check for updates

Citation: Okada, M.; Aoki, R.; Nakazawa, Y.; Tago, K.; Numata, K. CT and MR Imaging of Hepatocellular Carcinoma and Liver Cirrhosis. *Gastroenterol. Insights* **2024**, *15*, 976–997. https://doi.org/10.3390/gastroent15040068

Academic Editor: Jean-Francois H. Geschwind

Received: 19 September 2024
Revised: 15 October 2024
Accepted: 16 October 2024
Published: 5 November 2024

Copyright: © 2024 by the authors. Licensee MDPI, Basel, Switzerland. This article is an open access article distributed under the terms and conditions of the Creative Commons Attribution (CC BY) license (https://creativecommons.org/licenses/by/4.0/).

1. Introduction

Hepatocellular carcinoma (HCC) originates from the hepatocytes, and is the most common type of primary liver cancer. HCC is the fifth most common tumor in the world [1,2]. HCC has a complex pathogenesis, because HCC is induced by these etiologies, and is influenced by many risk factors. The molecular pathogenesis of HCC is still not completely understood. HCC is a heterogeneous malignant tumor that arises from a variety of causes of chronic liver damage, with viral hepatitis being the most common cause. Regardless of the cause, repeated hepatocellular damage leads to a vicious cycle of cell death and regeneration, and ultimately genomic instability, which is the final common pathway in the pathogenesis of HCC [3]. HCC typically develops in individuals with underlying liver disease, such as chronic hepatitis B or C infection, cirrhosis, non-alcoholic steatohepatitis (NASH), and long-term alcohol abuse. Thus, medical history, physical examination, and blood tests, such as alpha-fetoprotein levels and Protein Induced by Vitamin K Absence-II (PIVKA-II), are helpful in the diagnosis of HCC. Imagings, such as ultrasonography (US), computed tomography (CT), or magnetic resonance imaging (MRI) are involved in diagnosing the presence of HCC, differential diagnosis, and determining the efficacy of post-treatment HCC. US can be sensitive due to a high spatial resolution in detecting HCC, but this depends on the skill of the operator. Contrast-enhanced ultrasound (CEUS) has high temporal resolution and can delineate the delicate staining of liver tumors in real time. One of the characteristics of CEUS imaging is the sensitivity of the tumor enhancement in the arterial phase [4]. However, it has been suggested that CEUS findings may be confused with other liver diseases. Therefore, more accurate interpretation of CEUS imaging requires a combination of clinical information and other imaging findings, such as CT and MRI. CT is essential for the diagnosis of HCC, because of its high temporal resolution (short examination time) and ability to image a wide area, although radiation exposure is involved.

The role of CT for HCC is detecting the tumor, making a differential diagnosis, evaluating vascular invasion such as portal vein invasion, and evaluating distant metastases. The liver dynamic CT technique with a bolus injection of contrast media (CM) allows us to evaluate hemodynamics of the liver tumor and liver parenchyma. Four phases of liver dynamic CT, such as unenhanced, arterial, portal venous, and equilibrium phases, have substantially important roles in evaluating the hemodynamics of liver tumors compared to liver parenchyma, because the diagnosis of hypervascular HCC is based on arterial enhancement, followed by washout in the portal venous and/or equilibrium phase. According to the American Association for the Study of Liver Diseases (AASLD), a liver nodule larger than 1 cm in size in a cirrhotic liver that demonstrates the typical hemodynamics pattern on CT and MRI can be diagnosed as HCC without a biopsy. The Liver Imaging Reporting & Data System (LI-RADS®) is used as a system in patients for developing HCC, and this algorithm guides radiologists from benign to HCC. It was first published in 2006, and the latest version, v2018, includes CT/MRI, ultrasound, and treatment response criteria. This algorithm has been adopted as a diagnostic criterion by the AASLD, and is used in routine reports in the United States. The LI-RADS is expected to become an international standard in the imaging diagnosis of liver masses.

Liver cirrhosis (LC) can be evaluated using various imaging techniques. LC is established by a process of necrosis and regeneration of hepatocytes, resulting in fibrosis and capillarization of the hepatic sinusoids. Decreased liver parenchyma, impaired blood flow due to fibrosis and abnormal reconstruction, and hepatic arterial shunting result in portal hypertension, ascites, hepatic encephalopathy, lung damage, renal damage, cardiac damage, and hyponatremia. LC is associated with a high risk of developing HCC [5]. LC demonstrates less contrast enhancement of the liver than a normal liver, and sometimes shows inhomogeneous enhancement because of regeneration, fibrosis, and the altered portal venous flow. In addition, collateral vessels, such as paraumbilical vein, splenorenal shunt and esophageal varices, are seen due to portal hypertension. Ascites is also seen in patients with liver cirrhosis. LC is important in determining the strategy of HCC treatment, because many HCCs present with cirrhosis as the nativity of origin. The most commonly used imaging modalities to evaluate liver parenchyma are US, CT and MRI. US is non-invasive and readily available, and can show changes in liver texture, nodularity, and irregularity of the liver surface. The technique for measuring liver hardness with US, FibroScan, is a specialized ultrasound-based technique that measures liver stiffness to assess the degree of fibrosis in the liver. CT can show the decrease of liver volume, ascites and collateral blood vessel formation. Various evaluations by measuring liver and spleen volumes using CT volumetry (CTV) have also been proposed. MR Elastography (MRE) is also a non-invasive medical imaging technique used to assess the liver stiffness. It is particularly useful in diagnosing and staging liver diseases such as LC. MRE is used for the prediction of HCC occurrence and portal hypertension, the differentiation of benign/malignant liver lesions and HCC pathological grades, the prediction of post-treatment complications, the biomarker of treatment response, the prediction of HCC recurrence after treatment, the prediction of post-treatment complications, the biomarker of treatment response, and the prediction of HCC recurrence after treatment [6].

This review article presents the latest findings in the imaging diagnosis of HCC and LC, using current advanced CT and MRI to image liver lesions. To search for papers related to imaging techniques used in the diagnosis and management of HCC and liver cirrhosis, we used the search keywords HCC and liver fibrosis estimation in pubmed.

2. CT and MR Examinations of Liver Tumors

2.1. HCC Imaging on CT

CT is now widely available and represents an important modality to diagnose HCC and plan HCC therapy. Dynamic CT of the liver is performed by a bolus injection of iodine CM. A four-phase (unenhanced CT, arterial phase, portal venous, and equilibrium phase) protocol should be used to diagnose HCC. The arterial phase is divided into two phases [7],

an early arterial phase and a late arterial phase, in order to determine the preoperative vascular anatomy. The three dimensional (3D) image using the early arterial phase is useful to have as a strategy of preoperative anatomical evaluation for surgeons and as preoperative explanations for patients [8]. An intravenous bolus injection of contrast medium (CM) is essential for liver CT to diagnose HCC [9,10]. The diagnostic essential points for HCC are based on the hemodynamics pattern of dynamic CT, such as arterial hypervascularity (early stain) and washout at portal venous and/or equilibrium phases (Figure 1, Figure 2a). Up to the last 20 years, multidetector-row computed tomography (MDCT) has been playing an important role on HCC imaging because of higher spatial resolution, time resolution, reduced scan time, reduced motion artifact, and reduced radiation exposure. Diagnostic accuracy of the liver tumors has improved, because MDCT has higher spatial and temporal resolutions by the increase of both gantry rotation speed and the number of detector rows.

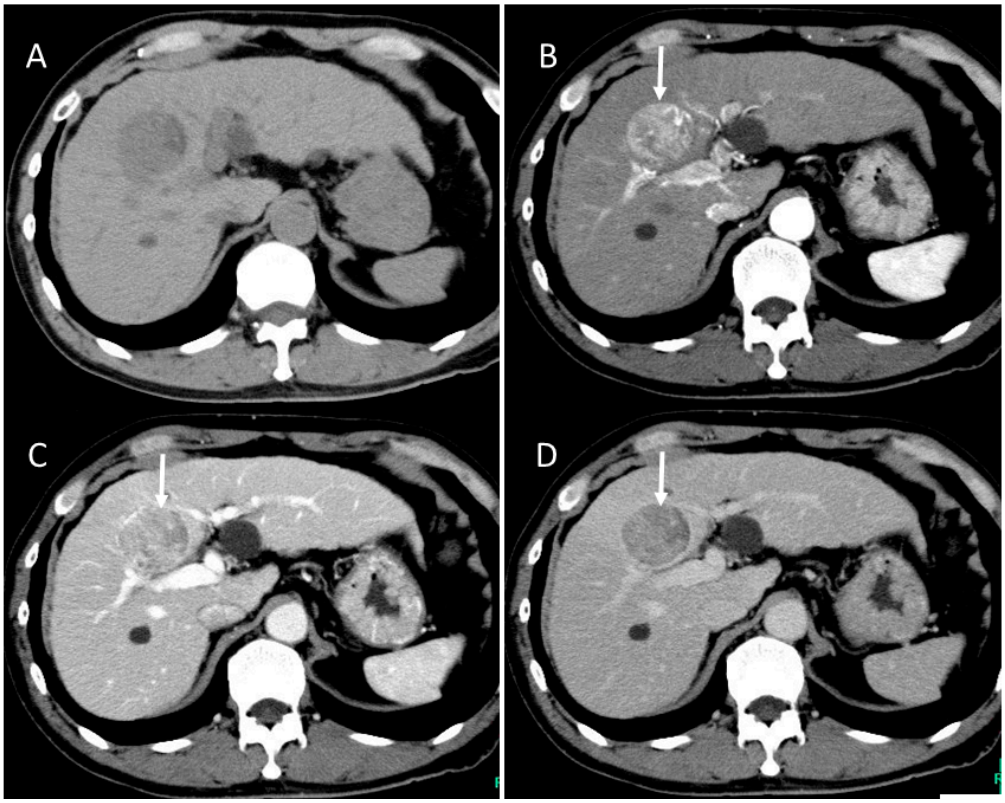
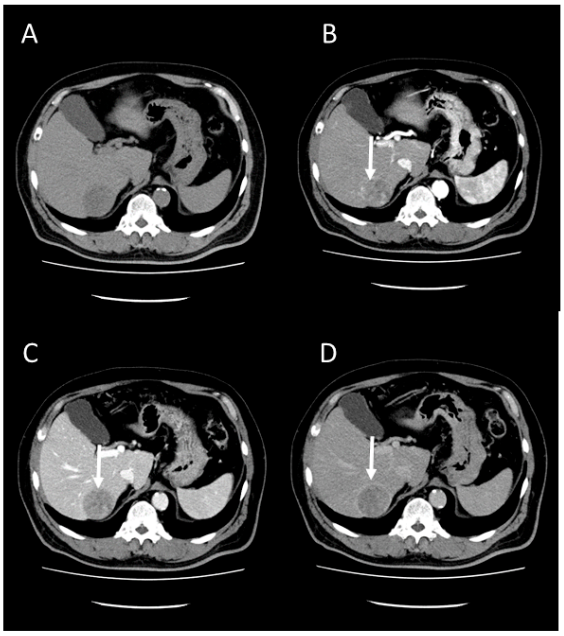
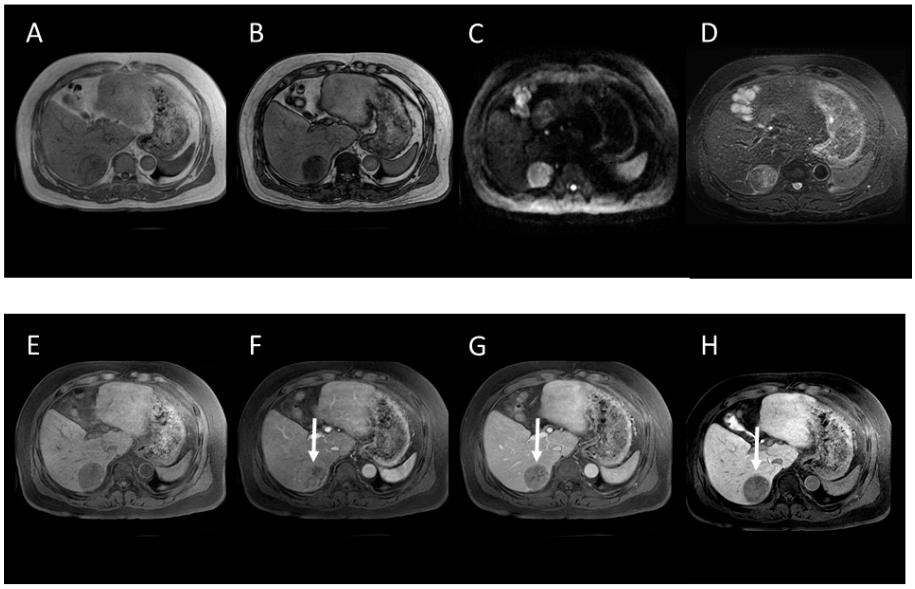


Figure 1. Hepatocellular carcinoma. Liver dynamic CT: (**A**) CT, unenhanced phase, (**B**) CT, arterial phase, (**C**) CT, portal venous phase, (**D**) CT, equilibrium phase. The intrahepatic tumor in liver segment 4/8, which shows low attenuation at the unenhanced phase, shows early stain in the arterial phase (arrow) and washout in the portal to the equilibrium phase (arrows). The tumor is surrounded by a capsule showing delayed enhancement with low attenuation in the arterial phase and high attenuation in the equilibrium phase.

Moreover, an advanced CT technology of dual energy CT has a high potential for liver imaging, including monochromatic images and CT dose reduction of radiation exposure. Photon counting CT [10–13] is one of the newest diagnostic imagings and is characterized by its ability to detect with high precision the X-ray energy change that occurs when X-rays penetrate a material, and to generate images based on that detection. High-energy resolution, low exposure, multi-energy imaging, low-contrast detection and reduced artifacts have been achieved. However, photon counting CT has just been clinically applied and is expected to develop in the future.



(**a**)



(**b**)

Figure 2. (**a**). **Hepatocellular carcinoma.** Liver dynamic CT: (**A**) CT, unenhanced phase, (**B**) CT, arterial phase, (**C**) CT, portal venous phase, (**D**) CT, equilibrium phase. The intrahepatic tumor in liver segment 7, which shows low attenuation at the unenhanced phase, shows early stain in the arterial phase (arrow) and washout in the portal to the equilibrium phase (arrows). The tumor is surrounded by a capsule showing delayed enhancement with low attenuation in the arterial phase and high attenuation in the equilibrium phase. (**b**). **Hepatocellular carcinoma.** EOB-MRI: (**A**), T1WI (in-phase), (**B**) T1WI (opposed phase), (**C**) DWI (b = 1000), (**D**) T2WI (fat saturation), (**E**) unenhanced phase, (**F**) arterial phase, (**G**) portal venous phase, (**H**) hepatocyte phase. On T1WI, the signal inside the intrahepatic tumor in liver segment 7 is slightly reduced from the in-phase to the opposed phase, suggesting fat content. DWI shows diffusion abnormality, and T2WI includes areas of high signal and areas of signal close to the liver parenchyma within the tumor. The intrahepatic tumor, which shows low attenuation at the unenhanced phase, shows early stain in the arterial phase (arrow), washout in the portal venous phase (arrow), and lower uptake of EOB in the hepatocyte phase (arrow).

2.2. HCC Imaging on MRI

Three major types of CMs used as liver-specific MRI are gadolinium-DTPA (Gd-DTPA), superparamagnetic iron oxide (SPIO) and gadoxetic acid (EOB) [14]. SPIO shows a high liver tumor detection capability because of its iron component, which shows the uptake into hepatic Kupffer cells and sinusoids. However, it is used less frequently in liver-specific MRI than EOB-MRI, because T2 weighted image (T2WI) sequences have a thicker slice thickness than 3D-T1WI under breath-hold imaging [15]. EOB-MRI has an important role for HCC diagnosis because of the evaluation of tumor vessels in the arterial phase and the uptake of hepatocytes in the hepatocyte phase [16]. HCC shows arterial phase hyperenhancement and washout. EOB-MRI is used to evaluate focal liver lesions, such as HCC, and HCC is normally hypointense to background liver on T1 weighted images (T1WI). EOB-MRI has a higher spatial resolution at the hepatocyte phase, because liver parenchymal enhancement by hepatocytes is obtained at 3D T1WI with a thinner slice thickness. EOB-MRI allows for superior lesion detection in early-stage HCC [15]. In EOB-MRI, there is no equilibrium phase in CT because of the distribution of the CM in the extracellular fluid and hepatocytes, although there is a time lag from the administration of the CM, which is referred to as the late phase at about 2 min after the start of the contrast. Thereafter, whether 5 or 15 min after the contrast has passed, it is called the hepatocyte phase, where the CM is distributed to the hepatocytes. EOB-MRI has similar imaging findings to CT in the arterial and portal phases for HCC imaging, but in the hepatocyte phase, HCC usually has a lower signal compared to the surrounding liver due to reduced hepatocyte function (Figure 2b). The uptake into HCC at the hepatocyte phase is seen when Organic anion-transporting polypeptide 8 or 1B3 (OATP8 or OATP1B3) is overexpressed (Figure 3), although many HCCs substantially show decreased uptake in the hepatocyte phase on EOB-MRI. The OATP8 or OATP1B3 expression and enhancement degree in hepatocellular nodules on EOB-MRI are correlated [17,18]. The expression of OATP8 or OATP1B3 determines the uptake of EOB-MRI in the hepatocyte phase in HCCs.

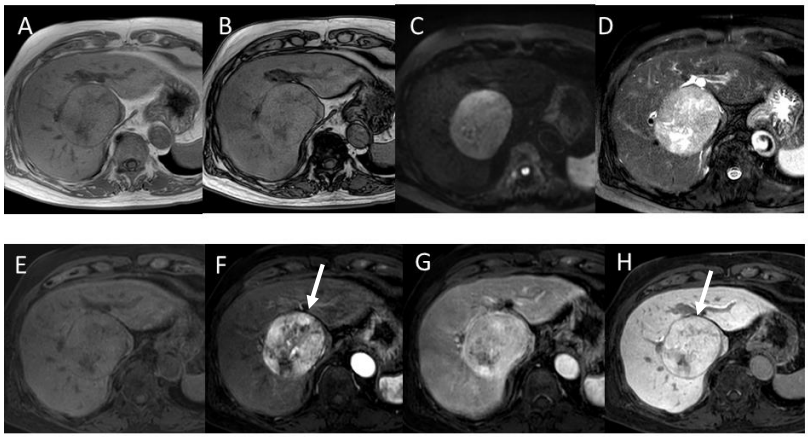


Figure 3. Hepatocellular carcinoma. EOB-MRI: (**A**) T1WI (in-phase), (**B**) T1WI (opposed phase), (**C**) DWI (b = 1000), (**D**) T2WI (fat saturation). (**E**) unenhanced phase, (**F**) arterial phase, (**G**) portal venous phase, (**H**) hepatocyte phase. T1WIs (in-phase and opposed phase) show no signal loss inside the intrahepatic tumor in liver segment 1 from the in-phase to the opposed phase. DWI shows diffusion abnormality, and T2WI includes areas of high signal and areas of signal close to the liver parenchyma within the tumor. The intrahepatic tumor, which shows low signal at the unenhanced phase, shows early stain in the arterial phase (arrow) and higher uptake of EOB in the hepatocyte phase (arrow).

The diffusion weighted image (DWI) of HCC with the apparent diffusion coefficient (ADC) is also characteristic and shows diffusion limitation, because abnormal diffusion in HCC causes high cell density, which restricts the movement of hydrogen protons in the extracellular fluid.

2.3. Liver Imaging Reporting and Data System (LI-RADS)

The LI-RADS® [19] was designed to standardize the interpretation and reporting of observations seen on studies performed in patients at risk of developing HCC. The LI-RADS® scale (LR-1, definitely benign; LR-2, probably benign; LR-3, intermediate probability of malignancy; LR-4, probably hepatocellular carcinoma [HCC]; LR-5, definitely HCC; LR-M, probably malignant but not HCC specific; and LR-TIV, tumor in vein) is a standardized system in patients for developing HCC [19].

The LI-RADS® also defines imaging time phases for CT and MRI. The arterial phase consists of early and late arterial phases [5]. The early arterial phase is a subtype in which the portal vein is not yet enhanced, whereas the late arterial phase is a subtype in which the portal vein is enhanced. The extracellular phase is a postcontrast phase in which liver enhancement is attributable mainly to the extracellular distribution of CM; both dynamic CT and EOB-MRI have this phase. The portal venous phase is the phase in which portal veins are fully enhanced, although hepatic veins are enhanced by antegrade flow. The delayed phase is acquired 2 to 5 min after the injection of CM, and portal and hepatic veins are enhanced but less than in the portal venous phase. The delayed phase is used for extracellular agents, but the transitional phase is used for EOB-MRI, typically acquired 2 to 5 min after the injection of CM. The hepatocyte phase is typically acquired about 15–20 min after the injection of CM. EOB-MRI is an imaging technique with a high capacity of small HCC detection, compared to liver dynamic CT [20], because Onishi et al. stated that EOB-MRI results in significantly improved sensitivity and diagnostic accuracy for the detection of hypervascular HCC, compared to liver dynamic CT. Images reflect pathology, and thus we should understand the findings of the intranodular blood supply of hepatic nodules on CT and MRI as references of multi-step hepatocarcinogenesis and multi-step change. The intranodular blood supply of hepatic nodules reflects the balance between the arterial flow and portal flow of the nodule [21].

Major imaging features of the LI-RADS® shows non-rim arterial phase hyperenhancement (APHE) in the arterial phase and non-peripheral washout in the portal venous or delayed phase. In addition, the enhancing capsule is visible as the enhancing rim in the portal venous phase, delayed phase, or transitional phase. Tumor size is also important in the diagnosis of HCC, and the LI-RADS® is only indicated as a major imaging feature for malignancy if the tumor is definitely a tumor and the size of a mass increases by $\geq$50% in $\leq$6 months.

2.4. American Association for the Study of Liver Diseases (AASLD)

The diagnostic algorithm for suspected HCC by the American Association for the Study of Liver Diseases (AASLD) guideline states that an imaging diagnosis of HCC should be made if a lesion larger than 1 cm shows a typical hypervascular enhancement pattern on a single dynamic imaging study (Figure 4) [22]. For hepatic nodules smaller than 1 cm, repeated sonography at 3 months is recommended to investigate the nodular size. Four-phase MDCT and dynamic contrast-enhanced MRI are recommended in this algorithm as imaging modalities to detect arterial hypervasculaity and washout at portal venous and/or equilibrium phases for hepatic nodules larger than 1 cm. Therefore, confirmation of arterial enhancement and the corresponding washout in the portal and equilibrium phases on dynamic CT is important to diagnose HCC after sonographic detection of hepatic nodules on the screening program. A biopsy is not needed to confirm the diagnosis of HCC if certain imaging criteria are met. Unfortunately, typical findings of HCC, such as arterial hypervascularity and washout at portal venous and/or equilibrium phases on liver dynamic CT, could not be obtained; other contrast-enhanced imagings or a biopsy of hepatic nodules are recommended.

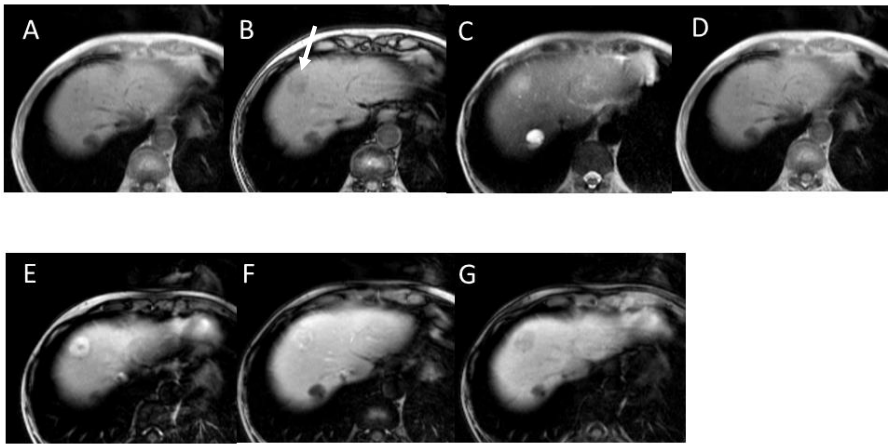


Figure 4. Hepatocellular carcinoma. EOB-MRI: (**A**) T1WI (in-phase), (**B**) T1WI (opposed phase), (**C**) DWI (b = 1000), (**D**) T2WI (fat saturation), (**E**) arterial phase, (**F**) portal venous phase, (**G**) hepatocyte phase. The intra-tumoral signal intensity decreased between in-phase and opposed phase (arrow) of T1WI. This patient received liver tumor biopsy, and the diagnosis of well-differentiated hepatocellular carcinoma was made.

3. Imaging Evaluation Methods for Cirrhosis and Other Diseases That Cause Liver Dysfunction

3.1. CT and MR Features of Liver Cirrhosis (LC)

In cirrhosis, irregularities of the hepatic margins may be seen, and splenomegaly may be present. Ascites and collateral veins may be seen, as well as a decrease in parenchymal contrast effect according to the progression of hepatic fibrosis, both in CT and MR.

A major problem in patients with LC is the increased susceptibility to HCC. One common hypothesis of hepatocarcinogenesis is that it is a "multi-step" process [23].

This mechanism envisages that HCC develops from cirrhotic or regenerative nodules (RNs) composed of proliferating hepatocytes. The increase in cell proliferation predisposes them to carcinogenic 'hits', thereby giving rise to cellular atypia (dysplastic foci). These RNs containing cellular or architectural atypia have been referred to as adenomatous hyperplasia, macroregenerative nodules, or dysplastic nodules (DNs). The diagnosis of these liver nodules may differ among pathologists. However, a hepatic nodule that has become hypervascularized is often considered a hepatic nodule to be treated in actual clinical practice.

3.2. Ultrasonography (US) and Magnetic Resonance Elastography (MRE)

Liver cirrhosis (LC) is one of the most important factors that leads to hepatocarcinogenesis. Cirrhotic liver shows limbal irregularity (Figure 5). LC leads to liver dysfunction, and various attempts have been made to perform liver function imaging. CT and MR studies are useful as additional information in the evaluation of liver function, but must be combined with other laboratory tests for a comprehensive evaluation. Liver function is affected by many factors and is not appropriate to be used alone.

LC is a late stage of the liver fibrosis caused by various factors, such as chronic alcohol abuse, viral hepatitis, and non-alcoholic fatty liver disease. Liver biopsy is the gold standard for diagnosing liver fibrosis, although it is invasive, and can be up to a 33% error in the diagnosis of LC [24]. This scarring disrupts the various functions of the liver. Imaging of LC refers to the use of various medical imaging techniques to visualize and assess the condition of the liver in individuals suspected or diagnosed with cirrhosis. Imaging plays an important role in diagnosing, staging, and monitoring the progression of LC. Ultrasonography (US) has a non-invasive character and FibroScan or Transient Elastography show an excellent ability of liver stiffness, such as the sensitivity of 96.2% and the specificity of 92.2% for fibrosis stage ≥ 4 [25]. MR Elastography (MRE) is also a non-invasive medical imaging technique used to assess the liver stiffness (Figure 6). MRE is used

for the prediction of HCC occurrence [26] and portal hypertension [27], the differentiation of benign/malignant liver lesions and HCC pathological grades, the prediction of post-treatment complications, the biomarker of treatment response, the prediction of HCC recurrence after treatment, the prediction of post-treatment complications, the biomarker of treatment response, and the prediction of HCC recurrence after treatment [6].

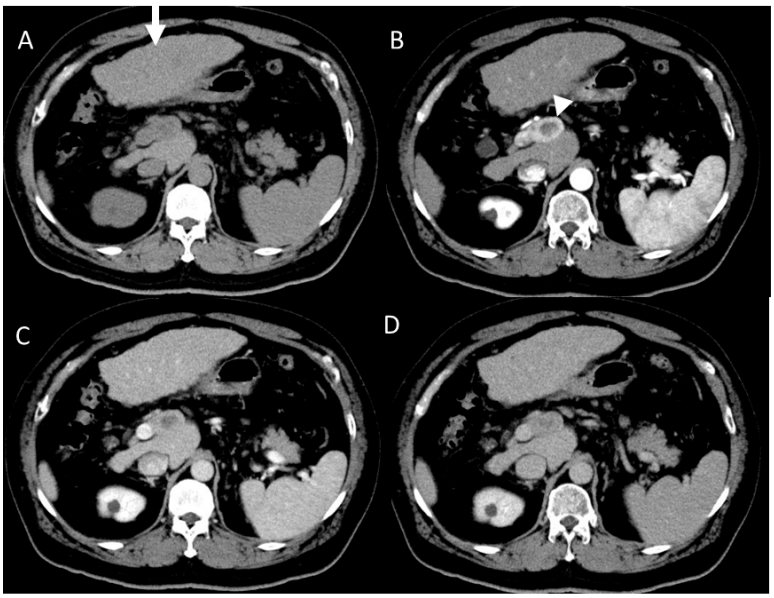


Figure 5. Liver cirrhosis. Liver dynamic CT: (**A**) unenhanced CT, (**B**) arterial phase CT, (**C**) portal venous phase CT, MRI, (**D**) equilibrium phase CT. An irregularity is seen at the hepatic margin (arrow). Less contrast enhancement of the liver is seen compared to normal liver. In this case, a hepatocellular carcinoma (arrowhead) is present as a protrusion from the caudate lobe of the liver. Splenomegaly is seen.

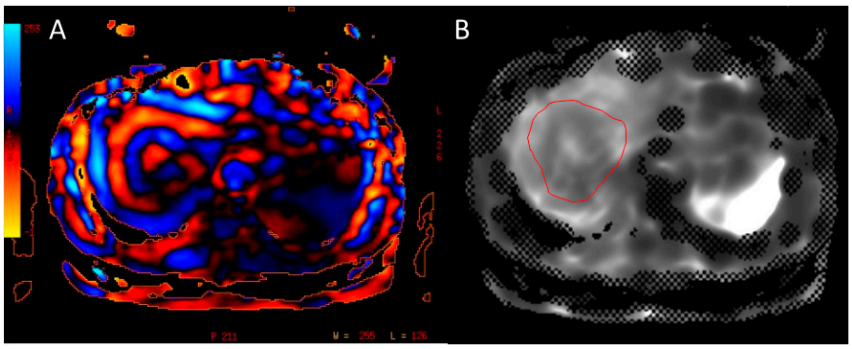


Figure 6. MR elastography (MRE). (**A**): Wave images reflecting phase differences (wave map), (**B**): monochrome display stiffness map (elastogram map). A 3.0-T-system (Discovery 750 W; GE Medical Systems) with a 32-channel-system (maximum gradient strength, 44 mT/m; peak slew rate, 200 T/m/s) and a phased-array coil is used for MRE in this case. For acquisition, low-frequency (60 Hz) mechanical shear waves (70% wave amplitude) are applied to the liver with a proprietary passive driver placed over the right upper quadrant of the abdominal wall. A two-dimensional spin-echo echo-planar imaging (SE-EPI) sequence (TR/TE 800/58.9 ms; matrix, 64 × 64; flip angle, 90 degrees; slice thickness, 7 mm; 80-Hz magnetization encoding gradient; bandwidth, 250 kHz; acquisition time, 22 s; number of slices, 4; field of view, 42 cm) was used to acquire magnitude and unwrapped phase difference wave images. Axial wave and elastogram map images were obtained to evaluate LSM using MR Touch software® device version (DV) 26.0 (GE Medical Systems). LSM was assessed by drawing freehand ROIs on the elastogram referring to the magnitude and wave images. The ROI was placed in the right lobe rather than the left lobe to avoid cardiac motion artifacts. Cross-hatching is an area where ROI should not be placed.

3.3. Technetium^{99m}galactosyl-Serum-Albumin (^{99m}Tc-GSA) Scintigraphy

^{99m}Tc-GSA scintigraphy, which can assess liver function, is compared to spleen volumetry for the assessment of liver fibrosis by Nakazawa et al. [28]. They state that both splenic volume to body surface area and GSA index have a high area under the curve (AUC, 0.83 for splenic volume to body surface, and 0.84 for GSA index) of the ROC analysis for severe fibrosis (≥F3–4). In addition, combined splenic volume to body surface, liver-to-spleen ratio on gadoxetate enhanced MRI, and hyaluronic acid correctly estimated severe LF, with an AUC of 0.91, which was significantly larger than the AUCs of the GSA index and the liver-to-spleen ratio or the liver-to-spleen ratio alone.

3.4. Extracellular Volume Fraction (ECV)

While these US and MRE techniques are certainly useful, there is renewed interest in liver and spleen volumetry [29–32], which is highly versatile and can be easily obtained with advances in workstations. These diagnostic methods are used to evaluate and monitor the progression of LC and provide a non-invasive way to assess the condition of the liver. The latest technological advances allow for a more accurate and sensitive estimation of LC [29]. Tago et al. [33]. stated that 90 consecutive patients were undergoing hepatectomy with CT volumetry (CTV) of the liver and spleen and extracellular volume fraction (ECV) of the liver in order to compare their ability to predict liver fibrosis (Figure 7). Results showed that splenic volume to body surface area (SV/BSA) was the better method in predicting liver fibrosis. ECV is also a promising candidate for estimating severe liver fibrosis. These results are expected to contribute to the safe operational management of liver resection surgery.

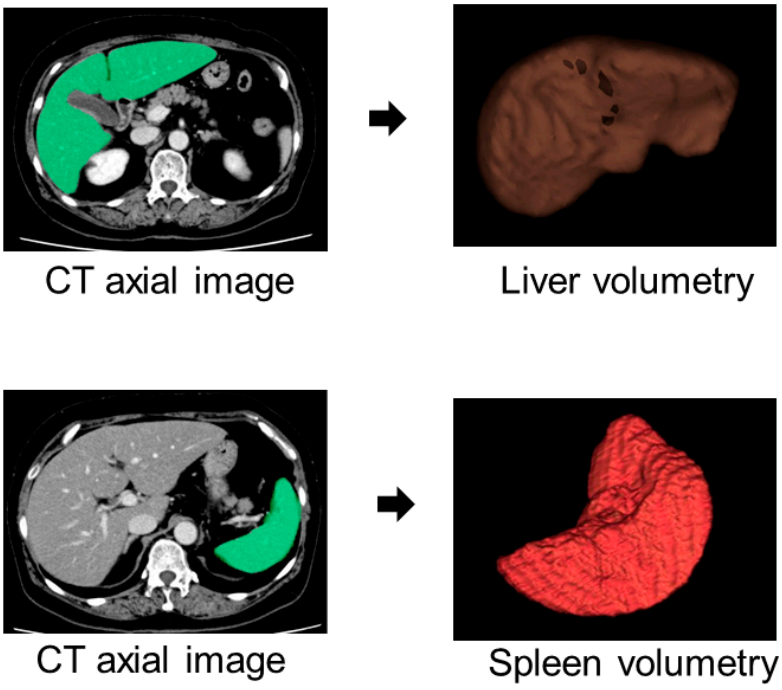


Figure 7. CT volumetry (CTV). CTV is generated from CT images by a workstation and semi-automatically measures liver and spleen volumes. An example is shown of the creation of liver and spleen volumetry using SYNAPSE VINCENT® version 5.5 (Fujifilm Medical).

3.5. Extracellular Volume Fraction (ECV)

Extracellular volume fraction (ECV) is the volume ratio of the extracellular fluid lumen in the tissue (Figure 8). The assessment of liver fibrosis to estimate ECV has been attempted utilizing the equilibrium phase on CT. ECV could be a reliable biomarker of liver fibrosis,

and an equilibrium phase delay time was set at 240 s after the CM injection [33,34], because liver fibrosis occurs in the extracellular space.

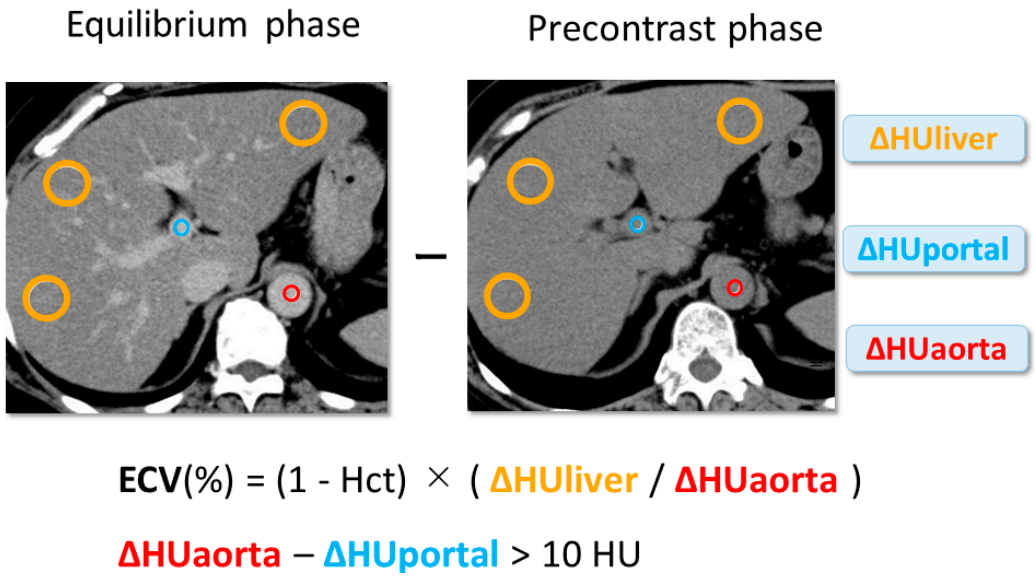


Figure 8. Extracellular volume fraction (ECV). ECV is calculated as ECV (%) = (1 − Hct) × ($\Delta HU_{liver}/\Delta HU_{aorta}$), where ΔHU = subtraction of unenhanced phase from equilibrium phase. To ensure a sufficient equilibrium phase, patients with significant differences between ΔHUaorta and ΔHUportal > 10 HU are excluded.

Tago et al. showed that splenic volume to body surface area is a better method for estimating LC grades, although manual-ECV has the ability to estimate cirrhosis (≥F4) [33]. In this paper, the authors compare the estimation ability of liver volume and spleen volume for liver fibrosis, and show that the spleen volume had a higher estimation ability for fibrosis, especially cirrhosis (≥F4). According to Tarao et al. [35], the patients with alcoholic liver fibrosis have increased liver volume because of the ballooning of hepatocytes along with an increased fibrotic component. Liver volume is affected by both hepatocyte changes associated with fibrosis and fibrosis of the liver parenchyma, which may differ from the perspective of liver stiffness.

3.6. Gadoxetic Acid Enhanced MRI (EOB-MRI)

Biochemical factors associated with liver enhancement on EOB-MRI were identified, with the goal of predicting the optimal time of the hepatobiliary phase in various clinical situations [36]. Study results revealed that the prothrombin (PT) activity, total bilirubin level, and total cholesterol level were associated with liver enhancement. It was also suggested that a PT activity of 86.9% or higher may reduce the examination time for EOB-MRI. EOB-MRI is a liver-specific contrast agent and can reflect liver function (Figure 9) [37,38]. The choice of imaging modality depends on factors such as the patient's overall health, the severity of cirrhosis, and the specific information needed by the healthcare provider to make clinical decisions.

The assessment of liver function by EOB-MRI showed that the use of the T1 relaxation time can be used to estimate liver function [37]. In this study, pre- and post-T1 relaxation times of the liver were measured to assess liver function through hepatocyte uptake and biliary excretion of EOB-MRI. Patients with cirrhosis showed significantly longer measurements before and after the T1 relaxation time compared to normal patients. It was also found that the rate of reduction in T1 relaxation time decreased with the progression of cirrhosis. These results suggest that T1 mapping using EOB is useful for assessing liver function.

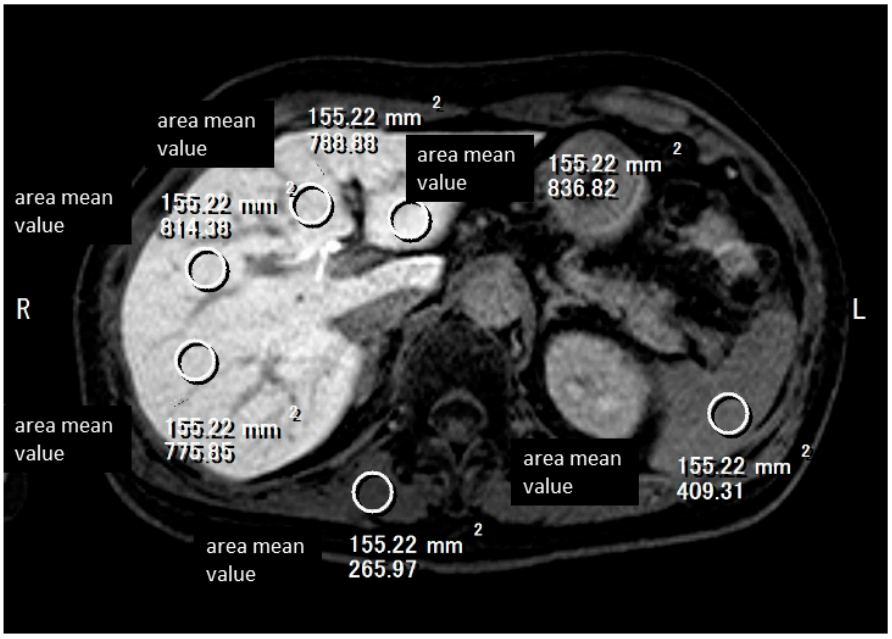


Figure 9. Gadoxetic acid enhanced MRI (EOB-MRI). In this example, four ROIs are placed within the liver parenchyma and the average value is calculated. The average signal value of the liver divided by the signal of the spleen is the liver–spleen ratio. The average signal value of the liver divided by the erector spinae signal is the liver–muscle ratio. The liver signal is considered to reflect liver function as it reflects the uptake of EOB into hepatocytes. Mean liver signal: (836 + 789 + 814 + 775)/4 = 803.5. Liver–spleen ratio: 803.5/266 = 3.02. Liver–muscle ratio: 803.5/409 = 1.96.

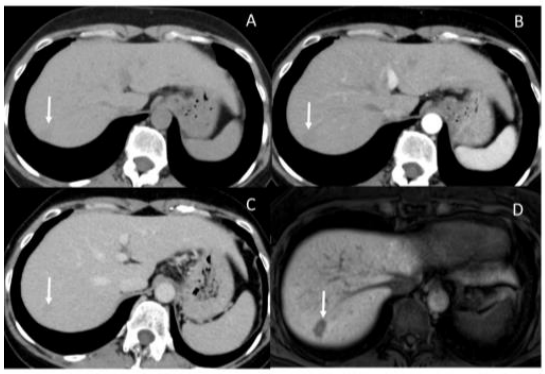
4. Hepatocellular Carcinoma (HCC) Imaging

4.1. Hepatocellular Carcinoma (HCC)

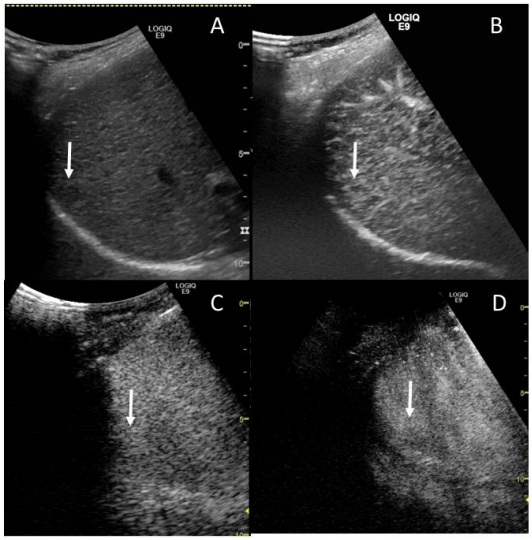
As the dysplastic nodule (DN), well-differentiated HCC (well-HCC), and moderately differentiated HCC (moderately differentiated HCC) portal venous blood flow decreases, the number of unpaired arteries increases [21]. However, the arterial blood supply decreases as poorly differentiated HCC (poorly HCC) in the late stage of HCC de-differentiation. Liver dynamic CT and EOB-MRI allow us to obtain the information regarding tumor vascularization, washout, and the capsule around the tumor. It can help to confirm the diagnosis of HCC. The appearance of HCC on CT depends on the tumor size and histologic tumor grades. The degree of uptake of CM in liver tumors on EOB-MRI is useful for estimating the degree of differentiation of HCC [39]. As the tumour dedifferentiates from DN, arterial blood flow temporarily decreases within the nodule, but then increases. On the other hand, portal blood flow decreases as the tumour dedifferentiates within the nodule. Early-stage hepatocellular carcinoma is a concept that differs from the pathological histological type, and the pathological image showing stromal infiltration is useful for diagnosis (Figure 10).

4.2. Early Hepatocellular Carcinoma (Early-HCC)

Early-HCCs refer to the initial stages of liver cancer when the tumor is localized and has not spread to distant parts of the liver or other organs. It means biologically early-stage cancer, which is a different concept from the classification of HCC according to the degree of differentiation as described below. Tumor cells of early-HCC grow in a replacing fashion, and portal tracts may be present in these lesions. The invasion into intralesional portal tracts, which is called a "stromal invasion", is important for the diagnosis of early HCC. Stromal invasion of early HCC has the active matrix metalloproteinase-1 (MMP-1) [40]. A decrease or disappearance of the ductalar reaction is also useful for the differentiation between early HCC from fibrosis with chronic hepatitis [41].



(**a**)



(**b**)

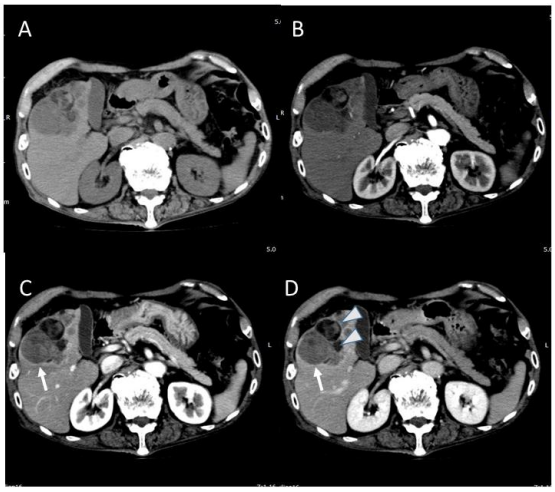
Figure 10. (**a**). **Early hepatocellular carcinoma**. Liver dynamic CT. (**A**); CT, unenhanced phase, (**B**); CT, arterial phase, (**C**); CT, equilibrium phase, (**D**); EOB-MRI hepatocyte phase. CT shows a low density tumor at unenhanced, arterial and equilibrium phase (arrows), and hepatocyte phase of EOB-MRI shows a lower intensity tumor (arrow), compared to surrounding liver parenchyma. (**b**). **Early hepatocellular carcinoma**. Contrast enhanced ultrasonography (CEUS). (**A**); Ultrasonography, B-mode, (**B**); CEUS, arterial phase, (**C**); CEUS, post-vascular phase (low MI), (**D**); CEUS, post-vascular phase (high MI), A small tumor in the liver segment 7 showed low-echoic mass at B-mode and iso-vascularity at arterial phase (arrow), and iso-echoic appearance at post-vascular phase (both low and high MI) (arrows). This patient received liver tumor biopsy, and the diagnosis of early hepatocellular carcinoma was made. Note; CEUS, contrast enhanced ultrasonography; MI, mechanical index.

Treatment of early-stage HCC is a potentially curative therapy with 5-year survival rates of 50–70% [42,43]. Early HCC substantially shows hypovascular tumors and slightly washouts on liver dynamic CT (Figure 10a). Hypovascular, iso-vascular, and hypervascular enhancements were observed in 50.0%, 17.3%, and 32.7% of early HCCs, respectively, at the arterial phase of CEUS (Figure 10b) [4].

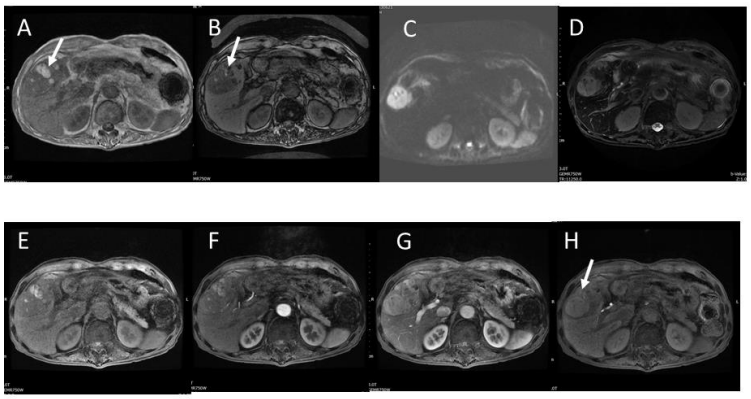
Angiogenesis, isoangiogenesis, and hyperangiogenesis were observed in 50.0%, 17.3%, and 32.7% of early-stage HCCs, respectively. Contrast-enhanced US was more sensitive than contrast-enhanced CT in detecting hyperangiogenesis in early-stage HCC. It may be difficult to differentiate early HCC from other benign lesions, such as RN and DN. A US-assisted biopsy of the lesion can be used to differentiate neoplastic lesions from non-neoplastic lesions.

4.3. Well-Differentiated Hepatocellular Carcinoma (Well-HCC)

The term "well-differentiated" indicates that the cancer cells closely resemble normal liver cells in terms of their structure and organization. Well-differentiated hepatocellular carcinomas (well-HCCs) have relatively low malignant potential, but rarely invade vessels or metastasis to other sites [44]. Microscopic invasion of stroma and portal tracts is the primary diagnostic feature to pathologically differentiate well-HCCs from DNs [45]. The diagnosis of well-HCC can be difficult, commonly requiring examination by several imaging modalities [46,47]. Fatty changes of tumor tissue were occasionally observed (Figure 11). Minimal enhancement of the tumor is substantially seen in well-differentiated HCC. Even though HCC is usually considered to be a hypervascular tumor, well-differentiated tumors can be hypovascular tumors.



(**a**)



(**b**)

Figure 11. (**a**). **Well-differentiated hepatocellular carcinoma.** Liver dynamic CT: (**A**) CT, unenhanced phase, (**B**) CT, arterial phase, (**C**) CT, portal venous phase, (**D**) CT, equilibrium phase. There are no apparent areas of early staining in the arterial phase, and the delayed enhancement is mainly on the capsule of the margins in the portal to the equilibrium phase (arrows). The internal structure of the tumor in liver S5 is heterogeneous, with areas of fat components (arrowheads). This patient received liver tumor biopsy, and the diagnosis of well-differentiated hepatocellular carcinoma was made. (**b**). **Well-differentiated hepatocellular carcinoma.** EOB-MRI: (**A**) T1WI (in-phase), (**B**) T1WI (opposed phase), (**C**) DWI (b = 1000), (**D**) T2WI (fat saturation), (**E**) unenhanced phase, (**F**) arterial phase, (**G**) portal venous phase, (**H**) hepatocyte phase. On T1WI, the signal inside the intrahepatic tumor in liver segment 5 is reduced from the in-phase to the opposed phase, suggesting fat components (arrows). DWI shows diffusion abnormality, and T2WI includes areas of high signal area within the tumor. The intrahepatic tumor, which shows high and low signals at the unenhanced phase, shows no apparent early stain in the arterial phase and uptake of EOB in the hepatocyte phase (arrow).

4.4. Moderately Differentiated Hepatocellular Carcinoma (Moderately HCC)

Dynamic CT substantially reveals a basket pattern which means hypervasculality of moderately differentiated hepatocellular carcinomas (moderately HCCs) (Figure 12). A peak of enhancement is usually seen at the arterial phase, followed by a rapid decrease of enhancement at the portal venous and equilibrium phases, because moderately HCC has a greater arterial blood supply [21]. Lesions larger than 3 cm show an often heterogeneous appearance, with a mosaic or mixed pattern arising from intra-tumoral necrosis, hemorrhage, fatty deposit, and interstitial fibrosis.

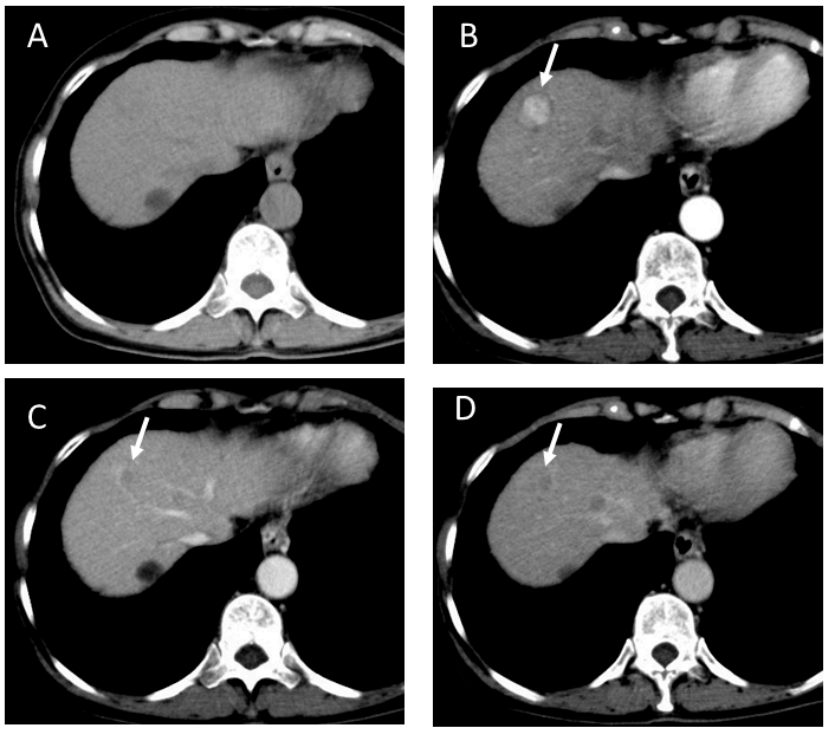


Figure 12. Moderately differentiated hepatocellular carcinoma. Liver dynamic CT: (**A**) CT, unenhanced phase, (**B**) CT, arterial phase, (**C**) CT, portal venous phase, (**D**) CT, equilibrium phase. The intrahepatic tumor in liver segment 8, which shows iso attenuation at the unenhanced phase, shows early stain in the arterial phase (arrow) and washout in the portal to the equilibrium phase (arrows). The tumor is surrounded by a capsule showing delayed enhancement with low attenuation in the arterial phase and high attenuation in the equilibrium phase.

4.5. Poorly Differentiated Hepatocellular Carcinoma (Poorly HCC)

The arterial blood supply of poorly HCCs is lower than that of moderately HCCs by CT during hepatic angiography (CTHA) [48]. Poorly HCCs often already have washout in the portal phase, and the timing of washout is earlier than well-HCCs or moderately HCCs because of the larger size of the sinusoids and the faster blood flow through the sinusoids of poorly HCCs (Figure 13) [49]. Poorly HCCs contain fat more frequently than moderately HCCs due to hypoxia caused by reduced arterial blood flow [50].

4.6. Fibrolamellar Hepatocellular Carcinoma (FL-HCC)

FL-HCC is a very rare tumor that occurs in young adults with non-cirrhosis and is estimated to account for approx. 0.8% in a large retrospective cohort study with HCC [51]. It is distinct from the more common HCC in terms of its clinical and pathological features. FL-HCC is a solitary mass with a fibrous capsule that is clearly distinguished from the surrounding liver. Furthermore, FLHCC is considered to have a better prognosis in comparison to HCC and intrahepatic cholangiocarcinoma [52]. Imaging findings may show

the central scar as hypoattenuation on CT, with hyperattenuation indicating calcification within the scar (Figure 14).

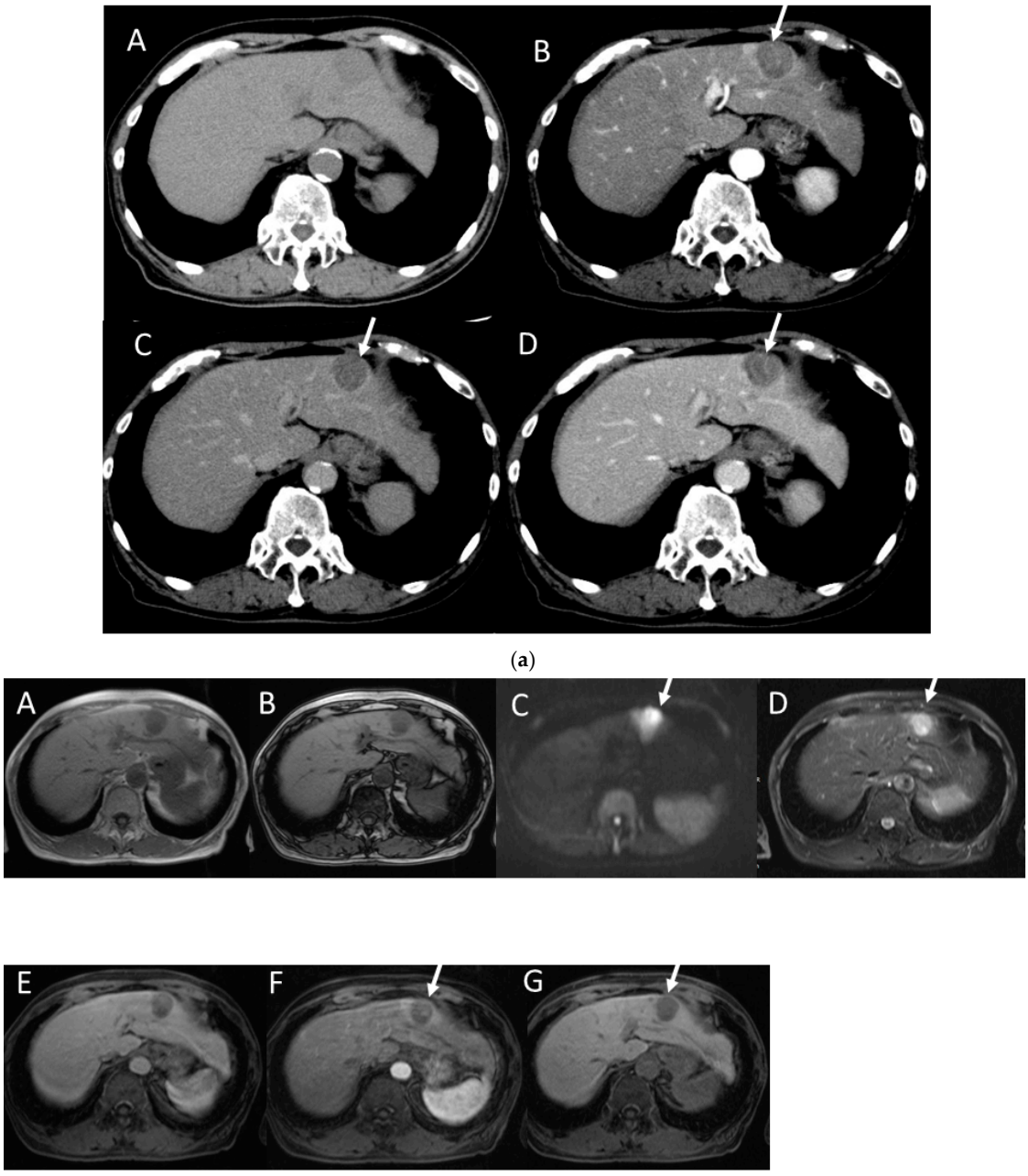


Figure 13. (**a**). **Poorly differentiated hepatocellular carcinoma.** Liver dynamic CT: (**A**) CT, unenhanced phase, (**B**) CT, arterial phase, (**C**) CT, portal venous phase, (**D**) CT, equilibrium phase. Dynamic CT of the liver shows a hypovascular tumor (arrow) in the liver segment S3. The tumor shows hypoattenuation compared to the surrounding liver, even in portal and equilibrium phases (arrows). (**b**). **Poorly differentiated hepatocellular carcinoma.** EOB-MRI: (**A**) T1WI (in-phase), (**B**) T1WI (opposed phase), (**C**) DWI (b = 1000), (**D**) T2WI (fat saturation), (**E**) unenhanced phase, (**F**) arterial phase, (**G**) hepatocyte phase. The arterial phase shows a hypovascular tumor (arrow), and the hepatocyte phase has a more prominent low signal than the surrounding liver (arrow). DWI shows strong diffusion abnormality (arrow), and T2WI shows high signal (arrow).

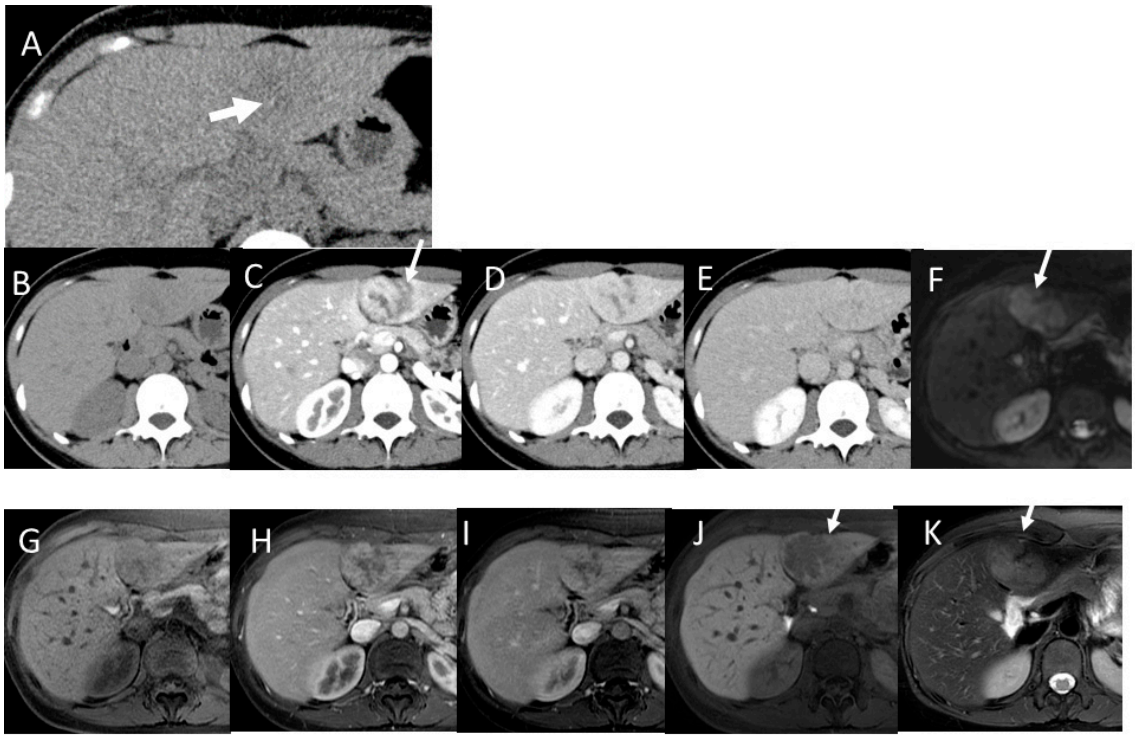


Figure 14. Fibrolamellar hepatocellular carcinoma. Liver dynamic CT: (**A**) CT, unenhanced phase (enlargement), (**B**) CT, unenhanced phase, (**C**) CT, arterial phase, (**D**) CT, portal venous phase, (**E**) CT, equilibrium phase, (**F**) DWI, (**G**) unenhanced phase, (**H**) arterial phase, (**I**) portal venous phase, (**J**) hepatocyte phase, (**K**) T2WI (fat saturation). A non-contrast CT shows a small calcification within the tumor (arrow). Dynamic contrast-enhanced CT shows early staining and heterogeneous washout of the tumor (arrows). The tumor shows diffusion abnormality (arrow) on MRI and a mild high signal on T2WI (arrow); EOB contrast-enhanced MRI shows early staining and reduced uptake (arrow) in the hepatocyte phase.

4.7. Combined Hepatocellular and Cholangiocarcinoma (cHCC-CCA)

Combined hepatocellular and cholangiocarcinoma (cHCC-CCA) is a rare type of primary liver cancer that exhibits features of both hepatocellular carcinoma (HCC) and cholangiocarcinoma (CCA). Age, gender, viral hepatitis status, and cirrhosis of cHCC-CCA are similar to HCC rather than CCA [53,54].

They are classified into the following categories: intermediate type of cells that are immunohistologically positive for both hepatocyte and cholangiocyte markers, hepatic stem-cell-like cells expressing c-kit, and cholangiocarcinoma-like cells, but they may be mixed. The 2019 edition of the World Health Organization (WHO) [55] for HCC is based on the 2010 edition, in which cHCC-CCA in the WHO 2019 edition was defined as a typical subtype in the classical type, subtypes with stem-cell features in the WHO 2010 edition. The intermediate-cell subtype in subtypes with stem-cell features in the WHO 2010 edition is the same as in the 2019 edition. The cholangiocellular subtype in the WHO 2010 edition is classified in the 2019 edition as cHCC-CCA if there is a component of HCC, and small duct intrahepatic cholangiocarcinoma (iCCA), if there is no component of HCC.

Imaging of cHCC-CCA shows both HCC and intrahepatic cholangiocarcinoma findings within a single tumor, with the hepatocellular carcinoma component showing early staining with peritumoral enhancement and washout on dynamic contrast-enhanced CT or MRI (Figure 15), while the cholangiocarcinoma component is delayed enhancement [56].

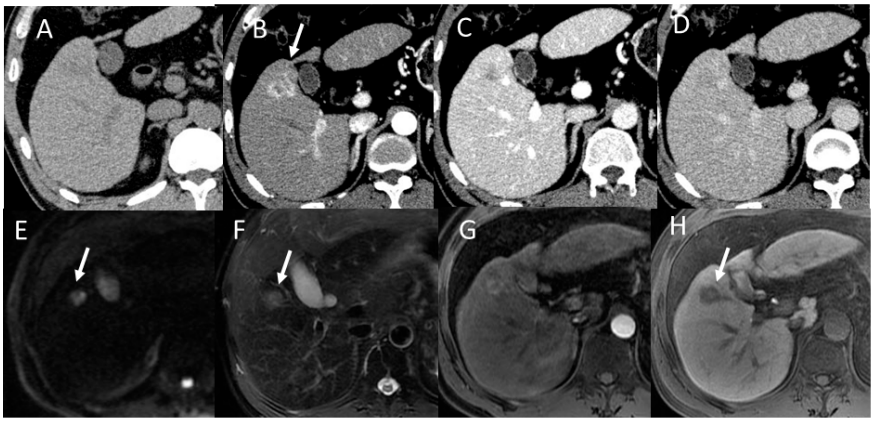


Figure 15. Combined hepatocellular and cholangiocarcinoma. Liver dynamic CT: (**A**) CT, unenhanced phase, (**B**) CT, arterial phase, (**C**) CT, portal venous phase, (**D**) CT, equilibrium phase, (**E**) DWI, (**F**) T2WI, (**G**) arterial phase, (**H**) hepatocyte phase. In the arterial phase, the margin of the tumor was stained in a ring shape (arrow). In the portal and equilibrium phase, the tumor is lower than that of the surrounding liver. The tumor shows diffusion abnormality and a mild high signal on T2WI (arrows); EOB contrast-enhanced MRI shows early staining and reduced uptake in the hepatocyte phase (arrow).

4.8. Steatohepatitic HCC (SH-HCC)

Steatohepatitic hepatocellular carcinoma (SH-HCC) is recognized as an HCC subtype, in the WHO Classification 2019. Pathologically, it is a steatohepatitic deposition [57]. Clinical features are the background metabolic syndrome and fatty hepatitis with heavy alcohol consumption. The tumor cells have similar features to those of fatty hepatitis, as histological features. SH-HCC contains a low attenuation suggestive of fat on non-enhanced CT and shows early staining and washout in the arterial phase, resulting in an image that resembles moderately differentiated hepatocellular carcinoma, with fat (Figure 16). A single-center retrospective study including 297 surgically resected HCCs found 5-year survival rates to be similar for SH-HCC and non-SH-HCC. The proportion of SH component recurrence-free survival (RFS) and 5-year overall survival (OS) did not affect OS and RFS [58].

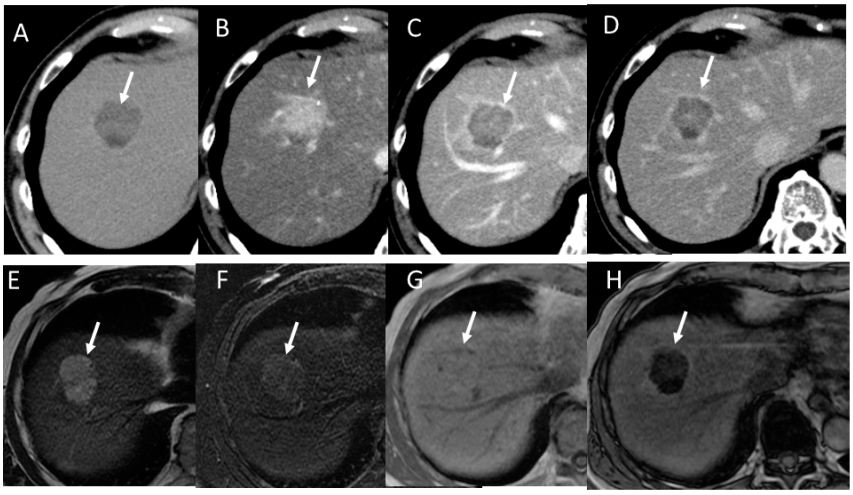


Figure 16. Steatohepatitic HCC (SH-HCC): (**A**) CT, unenhanced phase, (**B**) CT, arterial phase, (**C**) CT, portal venous phase, (**D**) CT, equilibrium phase, (**E**) T2WI, (**F**) T2WI (fat saturation), (**G**) T1WI (in-phase), (**H**) T1WI (opposed phase). Tumor in liver S8 contains low attenuation suggestive of fat on unenhanced CT (arrow), shows early staining in arterial phase (arrow) and washout is seen at portal venous phase and equilibrium phase (arrows); MRI of T2WI (arrow) shows reduced tumor (suggesting fat component) at fat-suppressed T2WI (arrow). T1WI shows that the signal reduction (suggestive of fat component) from in-phase (arrow) to opposed phase (arrow).

5. Conclusions

The imaging findings of HCC and liver parenchymal changes, including cirrhosis, were described. It should be understood that liver tumors and liver parenchyma are interrelated and that the contrast between liver tumors with and without parenchymal changes is variable.

The most appropriate and effective approach for the diagnosis of liver tumors is to make an individualized decision for each case. First, the patient's clinical information is evaluated, taking into account the patient's history, symptoms, and blood test results. Next, the imaging findings of CT and MRI are compared with and complemented by the results of other imaging studies to make a more accurate diagnosis.

Additional testing and evaluation may also be necessary if the imaging studies (e.g., MRI or CT) can be confused with other liver diseases. This may include a liver biopsy. These additional tests and evaluations are important to make a more definitive diagnosis [28,29,59–61].

When considering the cost of medical care, the optimal approach to HCC imaging diagnosis is to perform the minimum necessary tests. In addition, as a future research direction, it is important to establish imaging diagnosis of liver function necessary for treatment intervention, while performing imaging evaluation of the liver parenchyma together with tumour diagnosis. Familiarity with these specific CT and MRI features of liver tumors is beneficial to radiologists, as appropriate diagnoses can help avoid unnecessary invasive treatments. At present, it seems that the artificial intelligence (AI) diagnosis of HCC and cirrhosis is not yet at a level that can be used in daily clinical practice, but we are looking forward to future developments.

Author Contributions: Conceptualization, M.O. and K.N.; methodology, M.O.; software, M.O.; validation, M.O.; formal analysis, M.O.; investigation, M.O., R.A., K.T., Y.N. and K.N.; resources, M.O. and K.N.; data curation, M.O., R.A., K.T., Y.N. and K.N.; writing—original draft preparation, M.O.; writing—review and editing, M.O.; visualization, M.O.; supervision, K.N.; project administration, M.O. All authors have read and agreed to the published version of the manuscript.

Funding: This research received no external funding.

Institutional Review Board Statement: Not applicable.

Informed Consent Statement: Not applicable.

Data Availability Statement: Not applicable.

Conflicts of Interest: The authors declare no conflict of interest.

Abbreviations

ADC	apparent diffusion coefficient
APHE	arterial phase hyperenhancement
BSA	body surface area
CEUS	contrast-enhanced ultrasound
CM	contrast media
cHCC-CCA	combined hepatocellular and cholangiocarcinoma
CT	computed tomography
CTV	CT volumetry
DN	dysplastic nodule
DWI	diffusion weighted image
FL-HCC	fibrolamellar hepatocellular carcinoma
ECV	extracellular volume fraction
EOB	gadoxetic acid
HCC	Hepatocellular carcinoma
LC	liver cirrhosis
LI-RADS	Liver Imaging Reporting & Data System
MMP-1	matrix metalloproteinase-1
Moderately HCC	moderately differentiated HCC

MRI	magnetic resonance imaging
MRE	MR Elastography
OATP8	Organic anion-transporting polypeptide 8
OATP1B3	Organic anion-transporting polypeptide 1B3
OS	overall survival
Poorly HCC	Poorly differentiated HCC
RN	regenerative nodule
RFS	recurrence-free survival (RFS)
SPIO	superparamagnetic iron oxide
SH-HCC	steatohepatitic HCC
SV	splenic volume
T1WI	T1 weighted image
T2WI	T2 weighted image
US	ultrasonography
WHO	World Health Organization
^{99}mTc-GSA	Technetium 99 mg alactosyl-serum-albumin

References

1. Bosch, F.X.; Ribes, J.; Diaz, M.; Cleries, R. Primary liver cancer: Worldwide incidence and trends. *Gastroenterology* **2004**, *127*, S5–S16. [CrossRef] [PubMed]
2. Marrero, J.A.; Welling, T. Modern diagnosis and management of hepatocellular carcinoma. *Clin. Liver Dis.* **2009**, *13*, 233–247. [CrossRef] [PubMed]
3. Dhanasekaran, R.; Bandoh, S.; Roberts, L.R. Molecular pathogenesis of hepatocellular carcinoma and impact of therapeutic advances. *F1000Research* **2016**, *5*, 879. [CrossRef] [PubMed]
4. Numata, K.; Fukuda, H.; Miwa, H.; Ishii, T.; Moriya, S.; Kondo, M.; Nozaki, A.; Morimoto, M.; Okada, M.; Takebayashi, S.; et al. Contrast-enhanced ultrasonography findings using a perflubutane-based contrast agent in patients with early hepatocellular carcinoma. *Eur. J. Radiol.* **2014**, *83*, 95–102. [CrossRef] [PubMed]
5. Yoshiji, H.; Nagoshi, S.; Akahane, T.; Asaoka, Y.; Ueno, Y.; Ogawa, K.; Kawaguchi, T.; Kurosaki, M.; Sakaida, I.; Shimizu, M.; et al. Evidence-based clinical practice guidelines for Liver Cirrhosis 2020. *J. Gastroenterol.* **2021**, *56*, 593–619. [CrossRef]
6. Liang, J.; Ampuero, J.; Castell, J.; Zhang, Q.; Zhang, S.; Chen, Y.; Romeo-Gomez, M. Clinical application of Magnetic resonance elastography in hepatocellular carcinoma: From diagnosis to prognosis. *Ann. Hepatol.* **2023**, *28*, 100889. [CrossRef]
7. Murakami, T.; Kim, T.; Takamura, M.; Hori, M.; Takahashi, S.; Federle, M.P.; Tsuda, K.; Osuga, K.; Kawata, S.; Nakamura, H.; et al. Hypervascular hepatocellular carcinoma: Detection with double arterial phase multi-detector row helical CT. *Radiology* **2001**, *218*, 763–767. [CrossRef]
8. Takahashi, S.; Murakami, T.; Takamura, M.; Kim, T.; Hori, M.; Narumi, Y.; Nakamura, H.; Kudo, M. Multi-detector row helical CT angiography of hepatic vessels: Depiction with dual-arterial phase acquisition during single breath hold. *Radiology* **2002**, *222*, 81–88. [CrossRef]
9. Murakami, T.; Onishi, H.; Mikami, K.; Iannacone, R.; Federle, M.P.; Kim, T.; Hori, M.; Okada, A.; Marukawa, T.; Higashihara, H.; et al. Determining the optimal timing for early arterial phase hepatic CT imaging by measuring abdominal aortic enhancement in variable contrast injection protocols. *J. Comput. Assist. Tomogr.* **2006**, *30*, 206–211. [CrossRef]
10. Noguchi, Y.; Murakami, T.; Kim, T.; Hori, M.; Osuga, K.; Kawata, S.; Kumano, S.; Okada, A.; Sugiura, T.; Nakamura, H. Detection of hepatocellular carcinoma: Comparison of dynamic MR imaging with dy-namic double arterial phase helical CT. *AJR Am. J. Roentgenol.* **2003**, *180*, 455–460. [CrossRef]
11. Racine, D.; Mergen, V.; Viry, A.; Frauenfelder, T.; Alkadhi, H.; Vitzthum, V.; Euler, A. Photon-Counting Detector CT for Liver Lesion Detection-Optimal Virtual Monoenergetic Energy for Different Simulated Patient Sizes and Radiation Doses. *Investig. Radiol.* **2024**, *59*, 554–560. [CrossRef] [PubMed]
12. Schoenbeck, D.; Pauline Haag, N.; Elias Michael, A.; Michael Woeltjen, M.; Boriesosdick, J.; Saeed, S.; Borggrefe, J.; Robert Kroeger, J.; Henning Niehoff, J. Dedicated virtual non-contrast images adapted for liver tissue in clinical photon counting CT improve virtual non-contrast imaging in various organs beyond the liver. *Eur. J. Radiol.* **2023**, *167*, 111031. [CrossRef] [PubMed]
13. Graafen, D.; Stoehr, F.; Halfmann, M.C.; Emrich, T.; Foerster, F.; Yang, Y.; Dueber, C.; Mueller, L.; Kloeckner, R. Quantum iterative reconstruction on a photon-counting detector CT improves the quality of hepatocellular carcinoma imaging. *Cancer Imaging* **2023**, *23*, 69. [CrossRef] [PubMed]
14. Ibrahim, M.A.; Hazhirkarzar, B.; Dublin, A.B. *Gadolinium Magnetic Resonance Imaging*; StatPearls: Treasure Island, FL, USA, 2018.
15. Okada, M.; Imai, Y.; Kim, T.; Kogita, S.; Takamura, M.; Kumano, S.; Onishi, H.; Hori, M.; Fukuda, K.; Hayashi, N.; et al. Comparison of enhancement patterns of histologically confirmed hepatocellular carcinoma between gadoxetate- and ferucarbotran-enhanced magnetic resonance imaging. *J. Magn. Reson. Imaging* **2010**, *32*, 903–913. [CrossRef] [PubMed]

16. Reimer, P.; Rummeny, E.J.; Shamsi, K.; Balzer, T.; Daldrup, H.E.; Tombach, B.; Hesse, T.; Berns, T.; Peters, P.E. Phase II clinical evaluation of Gd-EOB-DTPA: Dose, safety aspects, and pulse se-quence. *Radiology* **1996**, *199*, 177–183. [CrossRef]
17. Narita, M.; Hatano, E.; Arizono, S.; Miyagawa-Hayashino, A.; Isoda, H.; Kitamura, K.; Taura, K.; Yasuchika, K.; Nitta, T.; Ikai, I.; et al. Expression of OATP1B3 determines uptake of Gd-EOB-DTPA in hepatocellular carcinoma. *J. Gastroenterol.* **2009**, *44*, 793–798. [CrossRef]
18. Kitao, A.; Matsui, O.; Yoneda, N.; Nozaka, K.; Shinmura, R.; Koda, Y.; Kobayashi, S.; Gabata, T.; Zen, Y.; Yamashita, T.; et al. The uptake transporter OATP8 expression decreases during multistep hepatocarcino-genesis: Correlation with gadoxetic acid enhanced MR imaging. *Eur. Radiol.* **2011**, *21*, 2056–2066. [CrossRef]
19. Chernyak, V.; Fowler, K.J.; Kamaya, A.; Kielar, A.Z.; Elsayes, K.M.; Bashir, M.R.; Kono, Y.; Do, R.K.; Mitchell, D.G.; Signal, A.G.; et al. Liver Imaging Reporting and Data System (LI-RADS) Version 2018: Imaging of Hepatocellular Carcinoma in At-Risk Patients. *Radiology* **2018**, *289*, 816–830. [CrossRef]
20. Onishi, H.; Kim, T.; Imai, Y.; Hori, M.; Nagano, H.; Nakaya, Y.; Tsuboyama, T.; Nakamoto, A.; Tatsumi, M.; Kumano, S.; et al. Hypervascular hepatocellular carcinomas: Detection with gadoxetate disodium-enhanced MR imaging and multiphasic multidetector CT. *Eur. Radiol.* **2012**, *22*, 845–854. [CrossRef]
21. Hayashi, M.; Matsui, O.; Ueda, K.; Kawamori, Y.; Kadoya, M.; Yoshikawa, J.; Gabata, T.; Takashima, T.; Nonomura, A.; Nakanuma, Y. Correlation between the blood supply and grade of malignancy of hepatocellular nodules associated with liver cirrhosis: Evaluation by CT during intraarterial injection of contrast medium. *AJR Am. J. Roentgenol.* **1999**, *172*, 969–976. [CrossRef]
22. Bruix, J.; Sherman, M. Management of hepatocellular carcinoma: An update. *Hepatology* **2005**, *53*, 1020–1022. [CrossRef] [PubMed]
23. Sakamoto, M.; Hirohashi, S.; Shimosato, Y. Early stages of multistep hepatocarcinogenesis: Adenomatous hyperplasia and early hepatocellular carcinoma. *Hum. Pathol.* **1991**, *22*, 172–178. [CrossRef] [PubMed]
24. Afdhal, N.H.; Nunes, D. Evaluation of liver fibrosis: A concise review. *Am. J. Gastroenterol.* **2004**, *99*, 1160–1174. [CrossRef] [PubMed]
25. Hashemi, S.A.; Alavian, S.M.; Gholami-Fesharaki, M. Assessment of transient elastography (FibroScan) for diagnosis of fibrosis in non-alcoholic fatty liver disease: A systematic review and meta-analysis. *Casp. J. Intern. Med.* **2016**, *7*, 242–252.
26. Abe, H.; Midorikawa, Y.; Higaki, T.; Yamazaki, S.; Aramaki, O.; Nakayama, H.; Moriguchi, M.; Kanda, T.; Moriyama, M.; Okada, M.; et al. Magnetic resonance elastography-based prediction of hepatocellular carcinoma re-currence after curative resection. *Surgery* **2021**, *170*, 167–172. [CrossRef]
27. Navin, P.J.; Gidener, T.; Allen, A.M.; Takahashi, N.; Michael, N.; Torbenson, S.; Kamath, P.S.; Ehman, R.L.; Venkatesh, S.K. The Role of Magnetic Resonance Elastography in the Diagnosis of Noncirrhotic Portal Hypertension. *Clin. Gastroenterol. Hepatol.* **2020**, *18*, 3051–3053.e3052. [CrossRef]
28. Nakazawa, Y.; Okada, M.; Hyodo, T.; Tago, K.; Shibutani, K.; Mizuno, M.; Yoshikawa, H.; Abe, H.; Higaki, T.; Okamura, Y.; et al. Comparison between CT volumetry, technetium(99m) galactosyl-serum-albumin scintigraphy, and gadoxetic-acid-enhanced MRI to estimate the liver fibrosis stage in preoperative patients. *Eur. Radiol.* **2024**, *34*, 2212–2222. [CrossRef]
29. Bae, J.S.; Lee, D.H.; Yoo, J.; Yi, N.J.; Lee, K.W.; Suh, K.S.; Kim, H.; Le, K.B. Association between spleen volume and the post-hepatectomy liver failure and overall survival of patients with hepatocellular carcinoma after resection. *Eur. Radiol.* **2021**, *31*, 2461–2471. [CrossRef]
30. Obmann, V.C.; Marx, C.; Hrycyk, J.; Berzigotti, A.; Ebner, L.; Mertineit, N.; Gräni, C.H.; Heverhagen, J.T.; Christe, A.; Huber, A.T. Liver segmental volume and attenuation ratio (LSVAR) on portal venous CT scans improves the detection of clinically significant liver fibrosis compared to liver segmental volume ratio (LSVR). *Abdom. Radiol.* **2021**, *46*, 1912–1921. [CrossRef]
31. Chow, K.U.; Luxembourg, B.; Seifried, E.; Bonig, H. Spleen Size Is Significantly Influenced by Body Height and Sex: Establishment of Normal Values for Spleen Size at US with a Cohort of 1200 Healthy Individuals. *Radiology* **2016**, *279*, 306–313. [CrossRef]
32. Lotan, E.; Raskin, S.P.; Amitai, M.M.; Kleinbaum, Y.; Veitsman, E.; Weiss, P.; Cohen-Ezra, O.; Berdichevski, T.; Ben-Ari, Z. The Role of Liver Segment-to-Spleen Volume Ratio in the Staging of Hepatic Fibrosis in Patients with Hepatitis C Virus Infection. *Isr. Med. Assoc. J.* **2017**, *19*, 251–256. [PubMed]
33. Tago, K.; Tsukada, J.; Sudo, N.; Shibutani, K.; Okada, M.; Abe, H.; Ibukuro, K.; Higaki, T.; Takayama, T. Comparison between CT volumetry and extracellular volume fraction using liver dynamic CT for the predictive ability of liver fibrosis in patients with hepatocellular carcinoma. *Eur. Radiol.* **2022**, *32*, 7555–7565. [CrossRef] [PubMed]
34. Shinagawa, Y.; Sakamoto, K.; Sato, K.; Ito, E.; Urakawa, H.; Yoshimitsu, K. Usefulness of new subtraction algorithm in estimating degree of liver fibrosis by calculating extracellular volume fraction obtained from routine liver CT protocol equilibrium phase data: Preliminary experience. *Eur. J. Radiol.* **2018**, *103*, 99–104. [CrossRef] [PubMed]
35. Tarao, K.; Hoshino, H.; Motohashi, I.; Iimori, K.; Tamai, S.; Ito, Y.; Takagi, S.; Oikawa, Y.; Unayama, S.; Fujiwara, T.; et al. Changes in liver and spleen volume in alcoholic liver fibrosis of man. *Hepatology* **1989**, *9*, 589–593. [CrossRef] [PubMed]
36. Okada, M.; Nakamura, Y.; Kuwatsuru, R.; Nakamura, Y.; Isoda, Y.; Goshima, S.; Hanaoka, R.; Haradome, H.; Shinagawa, Y.; Kitao, A.; et al. Biochemical and Clinical Predictive Approach and Time Point Analysis of Hepatobiliary Phase Liver Enhancement on Gd-EOB-DTPA–enhanced MR Images: A multicenter study. *Radiology* **2016**, *281*, 474–483. [CrossRef]
37. Katsube, T.; Okada, M.; Kumano, S.; Hori, M.; Imaoka, I.; Ishii, K.; Kudo, M.; Kitagaki, H.; Murakami, T. Estimation of liver function using T1 mapping on Gd-EOB-DTPA-enhanced magnetic resonance imaging. *Investig. Radiol.* **2011**, *46*, 277–283. [CrossRef]

38. Tokorodani, R.; Kume, T.; Daisaki, H.; Hayashi, N.; Iwasa, H.; Yamagami, T. Combining 99mTc-GSA single-photon emis-sion-computed tomography and Gd-EOB-DTPA-enhanced magnetic resonance imaging for staging liver fibrosis. *Medicine* **2023**, *102*, e32975. [CrossRef]
39. Sano, K.; Ichikawa, T.; Motosugi, U.; Sou, H.; Muhi, A.M.; Matsuda, M.; Nakano, M.; Sakamoto, M.; Nakazawa, T.; Asakawa, M.; et al. Imaging study of early hepatocellular ccinoma: Usefulness of gadoxetic acid-enhanced MR imaging. *Radiology* **2011**, *261*, 834–844. [CrossRef]
40. Okazaki, I.; Wada, N.; Nakano, M.; Saito, A.; Takasaki, K.; Doi, M.; Kameyama, K.; Otani, Y.; Kubochi, K.; Niioka, M.; et al. Difference in gene expression for matrix metalloproteinase-1 between early and ad-vanced hepatocellular carcinomas. *Hepatology* **1997**, *25*, 580–584. [CrossRef]
41. Park, Y.N.; Kojiro, M.; Di Tommaso, L.; Dhillon, A.P.; Kondo, F.; Nakano, M.; Sakamoto, M.; Theise, N.D.; Roncalli, M. Ductular reaction is helpful in defining early stromal invasion, small hepatocellular carcinomas, and dysplastic nodules. *Cancer* **2007**, *109*, 915–923. [CrossRef]
42. Llovet, J.M.; Schwartz, M.; Mazzaferro, V. Resection and liver transplantation for hepatocellular carcinoma. *Semin. Liver. Dis.* **2005**, *25*, 181–200. [CrossRef] [PubMed]
43. Llovet, J.M.; Burroughs, A.; Bruix, J. Hepatocellular carcinoma. *Lancet* **2003**, *362*, 1907–1917. [CrossRef] [PubMed]
44. Sugihara, S.; Nakashima, O.; Kojiro, M.; Majima, Y.; Tanaka, M.; Tanikawa, K. The morphologic transition in hepatocellular carcinoma. A comparison of the individual histologic features disclosed by ultrasound-guided fine-needle biopsy with those of autopsy. *Cancer* **1992**, *70*, 1488–1492. [CrossRef] [PubMed]
45. Pathologic diagnosis of early hepatocellular carcinoma: A report of the international consensus group for hepatocellular neo-plasia. *Hepatology* **2009**, *49*, 658–664. [CrossRef] [PubMed]
46. Kim, M.J.; Choi, J.Y.; Chung, Y.E.; Choi, S.Y. Magnetic resonance imaging of hepatocellular carcinoma using contrast media. *Oncology* **2008**, *75* (Suppl. S1), 72–82. [CrossRef]
47. Imai, Y.; Murakami, T.; Yoshida, S.; Nishikawa, M.; Ohsawa, M.; Tokunaga, K.; Murata, M.; Shibata, K.; Zushi, S.; Kurokawa, M.; et al. Superparamagnetic iron oxide-enhanced magnetic resonance images of hepatocellular carcinoma: Correlation with histological grading. *Hepatology* **2000**, *32*, 205–212. [CrossRef]
48. Asayama, Y.; Yoshimitsu, K.; Nishihara, Y.; Irie, H.; Aishima, S.; Taketomi, A.; Honda, H. Arterial blood supply of hepatocellular carcinoma and histologic grading: Radi-ologic-pathologic correlation. *AJR Am. J. Roentgenol.* **2008**, *190*, W28–W34. [CrossRef]
49. Okamoto, D.; Yoshimitsu, K.; Nishie, A.; Tajima, T.; Asayama, Y.; Ishigami, K.; Hirakawa, M.; Ushijima, Y.; Kakihara, D.; Nakayama, T.; et al. Enhancement pattern analysis of hypervascular hepatocellular carcinoma on dy-namic MR imaging with histopathological correlation: Validity of portal phase imaging for predicting tumor grade. *Eur. J. Radiol.* **2012**, *81*, 1116–1121. [CrossRef]
50. Asayama, Y.; Nishie, A.; Ishigami, K.; Ushijima, Y.; Takayama, Y.; Okamoto, D.; Fujita, N.; Kubo, Y.; Aishima, S.; Yoshizumi, T.; et al. Fatty change in moderately and poorly differentiated hepatocellular carcinoma on MRI: A possible mechanism related to decreased arterial flow. *Clin. Radiol.* **2016**, *71*, 1277–1283. [CrossRef]
51. El-Serag, H.B.; Davila, J.A. Is fibrolamellar carcinoma different from hepatocellular carcinoma? A US population-based study. *Hepatology* **2004**, *39*, 798–803. [CrossRef]
52. Alshareefy, Y.; Shen, C.Y.; Prekash, R.J. Exploring the molecular pathogenesis, diagnosis and treatment of fibrolamellar hepato-cellular carcinoma: A state of art review of the current literature. *Pathol. Res. Pract.* **2023**, *248*, 154655. [CrossRef] [PubMed]
53. Lee, W.S.; Lee, K.W.; Heo, J.S.; Kim, S.J.; Choi, S.H.; Kim, Y.I.; Joh, J.W. Comparison of combined hepatocellular and cholangiocar-cinoma with hepatocellular carci-noma and intrahepatic cholangiocarcinoma. *Surg. Today* **2006**, *36*, 892–897. [CrossRef]
54. Tang, D.; Nagano, H.; Nakamura, M.; Wada, H.; Marubashi, S.; Miyamoto, A.; Takeda, Y.; Umeshita, K.; Dono, K.; Monden, M. Clinical and pathological features of Allen's type C classification of resected combined hepatocellular and cholangiocarcinoma: A comparative study with hepatocellular carcinoma and cholangiocellular carcinoma. *J. Gastrointest. Surg.* **2006**, *10*, 987–998. [CrossRef] [PubMed]
55. Kim, T.H.; Kim, H.; Joo, I.; Lee, J.M. Combined Hepatocellular-Cholangiocarcinoma: Changes in the 2019 World Health Organiza-tion Histological Classification System and Potential Impact on Imaging-Based Diagnosis. *Korean J. Radiol.* **2020**, *21*, 1115–1125. [CrossRef] [PubMed]
56. Wang, X.; Wang, W.; Ma, X.; Lu, X.; Li, S.; Zeng, M.; Xu, K.; Yang, C. Combined hepatocellular-cholangiocarcinoma: Which preoperative clinical data and conven-tional MRI characteristics have value for the prediction of microvascular invasion and clinical significance? *Eur. Radiol.* **2020**, *30*, 5337–5347. [CrossRef]
57. Inui, S.; Kondo, H.; Tanahashi, Y.; Fukukura, Y.; Sano, K.; Morisaka, H.; Saito, K.; Kondo, F.; Fukusato, T.; Furui, S.; et al. Steatohepatitic hepatocellular carcinoma: Imaging findings with clinicopathological cor-relation. *Clin. Radiol.* **2021**, *76*, 160.e15–160.e25. [CrossRef]
58. Trapani, L.; Beaufrère, A.; Hobeika, C.; Codjia, T.; Albuquerque, M.; Bouattour, M.; Lesurtel, M.; Cauchy, F.; Paradis, V. Pathological overview of steatohepatitic hepatocellular carcinoma in a surgical series. *Histopathology* **2023**, *83*, 526–537. [CrossRef]
59. Mizuno, M.; Tago, K.; Okada, M.; Nakazawa, Y.; Arakane, T.; Yoshikawa, H.; Abe, H.; Matsumoto, N.; Higaki, T.; Okamura, Y.; et al. Extracellular volume by dual energy CT, hepatic reserve capacity scoring, CT. volumetry and Transient-elastographyfor estimating liver fibrosis. *Sci. Rep.* **2023**, *13*, 22038. [CrossRef]

60. Arakane, T.; Okada, M.; Nakazawa, Y.; Tago, K.; Yoshikawa, H.; Mizuno, M.; Abe, H.; Higaki, H.; Okamura, Y.; Takayama, T. Comparison between intravoxel incoherent motion and splenic volumetry to predict hepatic fibrosis staging in preoperative patients. *Diagnostics* **2023**, *13*, 3200. [CrossRef]
61. Nakazawa, Y.; Okada, M.; Tago, K.; Kuwabara, N.; Mizuno, M.; Abe, H.; Higaki, T.; Okamura, Y.; Takayama, T. Comparison between MR elastography and combination of CT, Gd-EOB-DTPAenhanced MRI and type IV collagen 7S for estimation of severe liver fibrosis in preoperative patients with hepatobiliary tumors. *Eur. Radiol.* 2024, *Online ahead of print*. [CrossRef]

Disclaimer/Publisher's Note: The statements, opinions and data contained in all publications are solely those of the individual author(s) and contributor(s) and not of MDPI and/or the editor(s). MDPI and/or the editor(s) disclaim responsibility for any injury to people or property resulting from any ideas, methods, instructions or products referred to in the content.